



Image quality and lesion detectability in low-dose pediatric ^{18}F -FDG scans using total-body PET/CT

Yu-Mo Zhao^{1,2} · Ying-He Li^{1,2} · Tao Chen^{1,2} · Wei-Guang Zhang^{1,2} · Lin-Hao Wang^{1,2} · Jiatai Feng³ · Chenwei Li³ · Xu Zhang^{1,2} · Wei Fan^{1,2} · Ying-Ying Hu^{1,2}

Received: 15 December 2020 / Accepted: 7 March 2021 / Published online: 18 March 2021

© The Author(s), under exclusive licence to Springer-Verlag GmbH Germany, part of Springer Nature 2021

Abstract

Purpose To investigate the effects of dose reduction on image quality and lesion detectability of oncological ^{18}F -FDG total-body PET/CT in pediatric oncological patients and explore the minimum threshold of administered tracer activity.

Methods A total of 33 pediatric patients (weight 8.5–58.5 kg; age 0.8–17.6 years) underwent total-body PET/CT using uEXPLORER scanner with an ^{18}F -FDG administered dose of 3.7 MBq/kg and an acquisition time of 600 s were retrospectively enrolled. Low-dose images (0.12–1.85 MBq/kg) were simulated by truncating the list-mode PET data to reducing count density. Subjective image quality was rated on a 5-point scale. Semi-quantitative uptake metrics for low-dose images were assessed using region-of-interest (ROI) analysis of healthy liver and suspected lesions and were compared with full-dose images. The micro-lesion detectability was compared among the dose-dependent PET images.

Results Our analysis shows that sufficient subjective image quality and lesion conspicuity could be maintained down to 1/30th (0.12 MBq/kg) of the administered dose of ^{18}F -FDG, where good image quality scores were given to 1/2- and 1/10- dose groups. The image noise was significantly more deranged than the overall quality and lesion conspicuity in 1/30- to 1/10-dose groups (all $p < 0.05$). With reduced doses, quantitative analysis of ROIs showed that SUV_{max} and SD in the liver increased gradually ($p < 0.05$), but SUV_{max} in the lesions and lesion-to-background ratio (LBR) showed no significant deviation down to 1/30-dose. One hundred percent of the ^{18}F -FDG-avid micro-lesions identified in full-dose images were localized down to 1/15-dose images, while 97% of the lesion were localized in 1/30-dose images.

Conclusion The total-body PET/CT might significantly decrease the administered dose upon maintaining the image quality and diagnostic performance of micro-lesions in pediatric patients. Data suggests that using total-body PET/CT, optimal image quality could be achieved with an administered dose-reduction down to 1/10-dose (0.37 MBq/kg).

Keywords Pediatric · Low-dose · Total-body PET/CT · ^{18}F -FDG

Introduction

Positron emission tomography coupled with computed tomography (PET/CT) has become an essential non-invasive

imaging method in oncology, providing both anatomic and metabolic features for clinical evaluations [1–3]. However, the administered activity of radiotracer and the acquisition time are often restricted by radiation safety and tolerance,

Yu-Mo Zhao and Ying-He Li contributed equally to this work.

This article is part of the Topical Collection on Dosimetry

✉ Xu Zhang
zhangx2@sysucc.org.cn

✉ Wei Fan
fanwei@sysucc.org.cn

✉ Ying-Ying Hu
huyy@sysucc.org.cn

¹ State Key Laboratory of Oncology in South China, Collaborative Innovation Center for Cancer Medicine, Guangzhou, Guangdong, China

² Department of Nuclear Medicine, Sun Yat-Sen University Cancer Center, 651 Dongfengdong Road, Guangzhou 510060, Guangdong, China

³ Central research institute, United Imaging Healthcare, Shanghai, China

especially for children [4, 5]. Pediatric patients with early exposure are at a higher risk of developing radiation-induced malignancies than adults, due to their developing bodies and greater life expectancies [6–9]. Therefore, minimizing the administered dose of radiotracer is of great importance in pediatric nuclear medicine. Studies have evaluated the radiotracer dose regimen for pediatric PET, especially for ^{18}F -Fluorodeoxyglucose (^{18}F -FDG), suggesting an optimized pediatric ^{18}F -FDG regimen of 3.2 MBq/kg for 5 min/bed or 5.3 MBq/kg for 3 min/bed with 15.7–18.0 cm axial field-of-view (FOV) [10–13]. Major imaging societies of North America, Europe, and Japan have presented recommendations, proposing that the administered dose of ^{18}F -FDG should be in a range of 3.5–5.3 MBq/kg for pediatric patients [14–19], with a minimum activity of 26 MBq for 2D and 14 MBq for 3D acquisitions. With the development of PET scanners, for instance, coincident photon-pair sensitivity and image reconstruction/processing algorithms, pediatric PET tracer dose could be reduced down to 1.5–1.8 MBq/kg using scanners with FOV of 25.0–25.8 cm [20, 21].

The dose of PET imaging is strongly related to the detection efficiency of the photon pairs emitted from positron-electron annihilation. The two primary parameters determining the detection efficiency of a PET scanner are the length of axial FOV and the sensitivity of the detector. Since 2005, almost all PET systems have been based on lutetium oxyorthosilicate scintillator for fully 3D mode data acquisition. For the PET scanner with an axial FOV length of 15–18 cm, approximately 1% of the photon emitted from a human body subjected radiotracer can be detected at any one time. A novel detector with a twofold increase in sensitivity of the current commercial detector emerged, and it has not yet been implemented in clinical systems for its lacking time-of-flight information [22]. Elongating the axial FOV length to 2 m allows a 40-fold increase in the detection efficiency of emitted photons in total-body PET imaging. The emergence of the state-of-the-art PET/CT scanner with 194-cm-long axial FOV provides an opportunity to further reduce acquisition duration and/or injected ^{18}F -FDG activity for pediatric patients [22–26]. A newly published study by Liu et al. on ultra-low-activity total-body dynamic PET imaging in 12 healthy adults concluded that total-body PET imaging allowed injected activity to be reduced down to 0.37 MBq/kg while maintaining ^{18}F -FDG kinetics and acceptable image contrast [26]. However, pediatric patients need to be separately evaluated due to their body weight and mass distribution.

Here, we aim to explore either the lowest possible dose regimen or the shortest acquisition time utilizing the uEXPLORER while maintaining the diagnostic quality of PET images, serving as a novel reference to pediatric PET studies and further investigations into ultra-low-dose or snapshot techniques. In this study, reduced ^{18}F -FDG doses were generated from randomized undersampling of the amount of

emitted photon counts from the list-mode PET data of full-dose images, where this method has been applied in previous studies in adults and infants [20, 25, 27, 28].

Materials and methods

Patients

In this retrospective study, consecutive pediatric patients who underwent total-body PET/CT at Sun Yat-Sen University Cancer Center from July 2020 to August 2020 were enrolled. The inclusion criteria were as follows: (1) under 18-years old and (2) body weight < 60 kg, where the exclusion criteria were (1) waiting time after ^{18}F -FDG injection ≥ 75 min, (2) diffuse liver involvement, and (3) without suspected FDG-avid lesion. The study was approved by the institutional review board of Sun Yat-Sen University Cancer Center, and the informed consent was obtained from all patients' legal guardians.

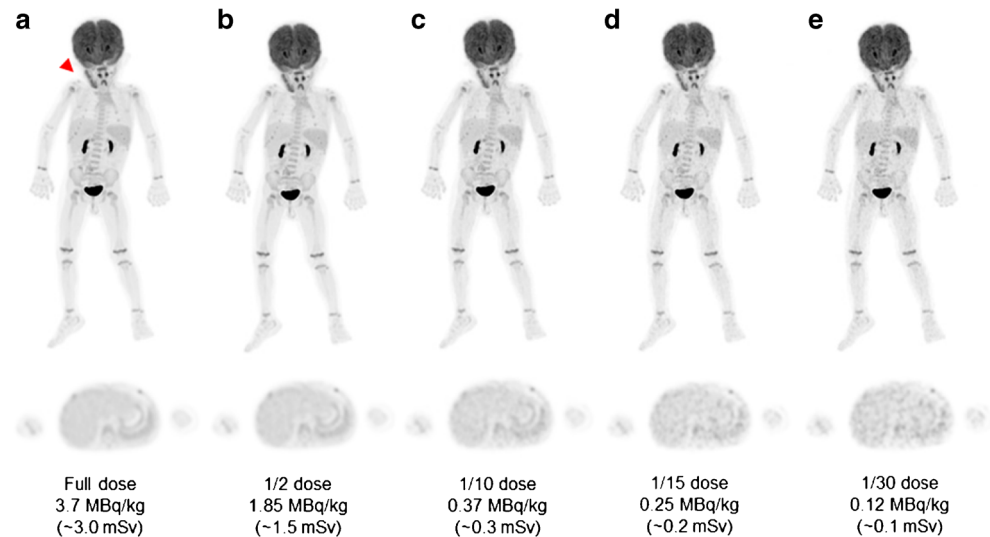
Imaging protocol

All patients fasted for 6 h before ^{18}F -FDG administration. The list-mode PET data were acquired using a total-body PET/CT scanner with 194-cm-long axial FOV (uEXPLORER, United Imaging Healthcare, Shanghai, China) 60 min after ^{18}F -FDG injection (3.7 ± 0.37 MBq/kg [0.1 ± 0.01 mCi/kg] activity per body weight). Low-dose CT scans of the whole body were obtained by uEXPLORER (tube current 10 mA, voltage 100 kV, rotation time 0.5 s, pitch 1.0125, collimation 80×0.5 mm) were reconstructed in a 512×512 matrix for attenuation correction. The acquisition time of emission images was 600 s, and PET images were reconstructed into 600, 300, 60, 40, and 20 s (Fig. 1). All PET images were reconstructed using ordered subset expectation maximization (OSEM) and setting a spectrum of parameters, for instance, time-of-flight and PSF modeling, 3 iterations, 20 subsets, matrix 256×256 , slice thickness of 2.89 mm, pixel size $2.34 \times 2.34 \times 2.89$ mm³ with a Gaussian post-filter (3 mm), and all necessary correction methods including attenuation and scatter correction. All image evaluation has been performed in a commercial medical image processing workstation (uWS-MI, United Imaging Healthcare).

Qualitative imaging assessment

The subjective PET image quality was independently rated on a 5-point Likert scale by 3 nuclear radiologists (a senior radiologist with > 8-year experience, a radiologist > 5-year experience, and a junior radiologist with 1 year of post-fellowship experience reading PET/CT scans) blinded to patient history and dose group of the images. Four simulated dosing levels

Fig. 1 ^{18}F -FDG PET image of a 1.9-year-old male patient weighted 10 kg with Langerhans cell histiocytosis was reconstructed into 600, 300, 60, 40, and 20 s shown in MIP and axial view (a–e), representing full dose, 1/2 dose, 1/10-dose, 1/15-dose, and 1/30-dose, respectively. The overall image scores of 5, 4, 3, and 2 were given to the group 300, 60, 40, and 20 s according to axial view images. Data in the parantheses were estimated effective dose



were included in the qualitative PET assessments (Fig. 1): 1.85 MBq/kg (1/2-dose, G300s), 0.37 MBq/kg (1/10-dose, G60s), 0.25 MBq/kg (1/15-dose, G40s), and 0.12 MBq/kg (1/30-dose, G20s). A 5-point Likert scale was used for (1) overall impression of the image quality, (2) conspicuity of the major suspected malignant lesions, and (3) image noise. The 5-point Likert scale for overall image quality comprises five categories which are defined as score (1) state-of-the-art quality, (2) superior to the regular image quality of daily practice, (3) equal to the regular quality of daily practice, (4) barely diagnostic, and (5) non-diagnostic (Supplementary Table 1). Among which, grade 3 indicates a quality of clinical routine image quality by a digital PET/CT scanner (FOV, 22.1 cm; acquisition time, 1.5–2.0 min/bed positions, 6–10 bed position/patient). Example images of grades 5–1 (5: excellent, 1: poor) have been illustrated in Fig. 1.

Quantitative imaging analysis

The objective image quality evaluation was performed by an experienced technician under the supervision of a radiologist. Three 2-dimensional circular region-of-interests (ROIs) with a diameter of 2 cm was drawn on a homogeneous area of the liver parenchyma, avoiding vessels and tumor. Liver semi-quantitative uptake measurements, including SUV_{max} , SUV_{mean} , and standard deviation (SD), were recorded. ^{18}F -FDG-avid suspected lesions (not necessarily malignant) with the shortest long-diameter were identified, and ROIs of such lesions were drawn on the slice where the diameter of the lesion maximized. The lesion-to-background ratio (LBR) was calculated as SUV_{max} of the lesion divided by the SUV_{mean} of the liver. The location of the lesion was confirmed on CT scan acquired with PET image, and the long diameter of the lesions on CT scans was measured after quality rating.

The corresponding locations of the micro-lesion identified on the PET images of G600s with standard administered dose were documented and served as a reference to estimate lesion detectability. Randomized orders of low-dose images were to minimize recall bias. Images with excessive background noise or poor image quality that made lesions un-diagnosable were documented.

Statistical analysis

The statistical analyses were performed using R statistical package. The Fleiss kappa test was used to measurement the inter-rater agreement for multiple raters. A kappa value of 0.41–0.60, 0.61–0.80, and 0.81–1.00 indicates moderate, substantial, and almost perfect agreement, respectively. Kruskal-Wallis rank-sum test and Dunn's post hoc test for multiple comparisons were applied in subjective image quality analyses between different subsets. To overcome the difference in SUV among patients due to individual metabolism, paired *t* test with Bonferroni correction was used to confirm the objectivity of image quality in different groups. SUV_{max} , SD, and LBR were calculated. $p < 0.05$ was considered as statistically significant.

Table 1 Patient characteristics

	Mean±SD	Range
Age (years)	8.3 ± 5.1	0.8–17.6
Weight (kg)	28.0 ± 16.6	8.5–58.5
Height (cm)	125.2 ± 31.2	70.0–176.0
Injected dose (MBq)	105.2 ± 60.6	32.9–217.9
Injected dose per weight (MBq/kg)	3.8 ± 0.2	3.18–4.26
Waiting time (min)	63 ± 7	48–74
Lesion size (mm)	8 ± 2	5–18

Results

Patients

A total of 33 pediatric oncological patients (24 males, 9 females), with a mean age of 8.3 years, ranging from 0.8 to 17.6 years, and a mean body mass index (BMI) of 16.2 kg/m², ranging from 12.2 kg/m² to 22.2 kg/m², were enrolled in this study (Table 1). Among all, 8 had lymphoma (7 non-Hodgkin lymphoma, 1 Hodgkin lymphoma), 10 had sarcoma (5 rhabdomyosarcoma, 2 Ewing sarcoma, 3 with other types), 7 had neuroblastoma, 3 had nasopharyngeal carcinoma, and 5 with other diseases.

Image quality

For the subjective study, the inter-rater agreements of Likert scoring were substantial for the overall image quality, lesion conspicuity, and image noise, with Fleiss kappa values of 0.769, 0.844, and 0.906, respectively. The subjective image quality scores were compared between G300 s, G60s, G40s, and G20s, where Table 2 listed the mean value \pm SD of Likert scoring. G300 s showed an excellent image quality with a grade of 5, for which all perspectives were scored in a range of 4–5. Overall image quality was 4.2 ± 0.4 for G60s, 3.4 ± 0.5 for G40s, and 2.2 ± 0.4 for G20s. Image noise of G60s, G40s, and G20s were scored 3.8 ± 0.4 , 3.0 ± 0.3 , and 2.0 ± 0.5 , respectively. For lesion conspicuity, it illustrated a similar variation tendency compared with image quality and noise (G60s, 4.0 ± 0.4 ; G40s, 3.7 ± 0.5 ; G20s, 2.7 ± 0.5). Between any two groups in reconstructed subsets (G300 s, G60s, G40s, and G20s), the scores of overall image quality, lesion conspicuity, and image noise were significantly different ($p < 0.001$ with/without Bonferroni correction), except for lesion conspicuity between G40s and G60s ($p < 0.037$ with Bonferroni correction).

The objective measurements of image quality, including SUV_{max}, and SD of the liver uptake, SUV_{max} and SD of the lesion uptake, and LBR were presented in Table 3. Measurements of G600s were served as reference. Changes from G600s to G300 s, G60s, G40s, G20s (Fig. 2) were calculated as subtracting the value of measurements in G600s

from that in the dose-reduced groups and noted as G300 s-G600s, G60s-G600s, G40s-G600s, and G20s-G600s.

The change in SUV_{max} of the liver increased gradually as the simulated dose was reduced. The liver SUV_{max} in G60s-G600s, G40s-G600s, and G20s-G600s were significantly higher than that of the G300 s-G600s ($p < 0.05$). The difference was not significant between G60s-G600s and G40s-G600s ($p = 1$ with Bonferroni correction). The SD of the liver uptake was significantly increased with simulated dose reduction ($p < 0.05$). The differences of changes in SUV_{max} of the lesions and LBR were not significant (all $p > 0.1$ with or without Bonferroni correction). The mean percent changes of LBR were 3.4–5.2% for G300 s-G600s, G60s-G600s, G40s-G600s and 11.5% for G20s-G600s. Details are listed in Supplementary Table 2.

Micro-lesion detectability

A total of 33 ¹⁸F-FDG-avid suspected micro-lesions with a mean diameter of 8 ± 2 mm were identified on the PET images of G600s. Among these lesions, there were 19 in the lymph node, 3 in the bone, 3 in the subcutaneous tissue, 2 in the liver, and 6 in the other organs, and details are provided in Supplementary Table 3. Example serial PET images of 2 micro-lesions are presented in Fig. 3. In G300 s, G60s, and G40s, all suspected micro-lesions were identified by all 3 radiologists, with a lesion detection rate of 100% relative to G600s. In G20s, 32 (97%) ROIs were identified by the 3 radiologists, where 1 lesion was missed (Fig. 3A) by all 3 radiologists.

Discussion

This study investigates image quality and micro-lesion detectability of dose-dependent PET images for total-body PET/CT scanner with a 194-cm-long axial FOV in pediatric patients. In this proof-of-concept study, our results from generated low-dose images suggested that an administered activity of 1/10-dose (0.37 MBq/kg) secures an optimal image quality superior to that of conventional digital PET; 1/15-dose (0.25 MBq/kg) showed a comparable image quality while maintaining PET parameters. Although the 1/30-dose (0.12 MBq/kg) PET images showed an arguably diagnostic image quality, the variations in PET parameters were unacceptable. Despite that the image noise increased more prominently than the overall image quality degradation as the dose decreased, micro-lesion detectability was minimally compromised.

As for the objective results, both SD and SUV_{max} in the liver increased gradually as the dose decreased; nevertheless, SUV_{mean} in the liver was relatively stable in between simulated dose reduction groups. This observation is consistent with the feature of background measurement, where the statistic

Table 2 Subjective image quality assessed by 5-point Likert scale

	Group 300s	Group 60s	Group 40s	Group 20s
Overall quality	4.9 ± 0.3	4.2 ± 0.4	3.4 ± 0.5	2.2 ± 0.4
Lesion conspicuity	5.0 ± 0.1	4.0 ± 0.3	3.7 ± 0.5	2.7 ± 0.5
Image noise	5.0 ± 0.1	3.8 ± 0.4	3.0 ± 0.3	2.0 ± 0.3

All scores were presented as mean value \pm SD and the images were reconstructed with a voxel size of $3.125 \times 3.125 \times 2.89$ mm³

Table 3 SUV, SD and LBR of the healthy liver and micro-lesions ($N=33$)

	Group 600s	Group 300s	Group 60s	Group 40s	Group 20s
Liver SUV _{max}	1.78 ± 0.49	1.85 ± 0.49	2.12 ± 0.56	2.22 ± 0.68	2.42 ± 0.77
Change of Liver SUV _{max}		0.07 ± 0.09	0.35 ± 0.23	0.45 ± 0.30	0.65 ± 0.40
Liver SD	0.05 ± 0.02	0.08 ± 0.03	0.19 ± 0.07	0.23 ± 0.09	0.32 ± 0.11
Change of Liver SD†		0.04 ± 0.03	0.14 ± 0.05	0.17 ± 0.08	0.26 ± 0.1
Lesion SUV _{max}	3.64 ± 1.68	3.89 ± 1.72	3.81 ± 1.81	3.81 ± 1.73	3.95 ± 1.75
Change of Lesion SUV _{max} †		0.12 ± 0.25	0.04 ± 0.4	0.03 ± 0.38	0.18 ± 0.59
Lesion SD	0.5 ± 0.27	0.55 ± 0.29	0.55 ± 0.32	0.57 ± 0.29	0.64 ± 0.34
Change of Lesion SD†		0.03 ± 0.07	0.04 ± 0.15	0.06 ± 0.12	0.13 ± 0.22
LBR	2.39 ± 1.29	2.51 ± 1.32	2.51 ± 1.47	2.56 ± 1.53	2.69 ± 1.66
Change of LBR†		0.12 ± 0.21	0.13 ± 0.32	0.13 ± 0.32	0.31 ± 0.65

All data were presented as mean ± SD

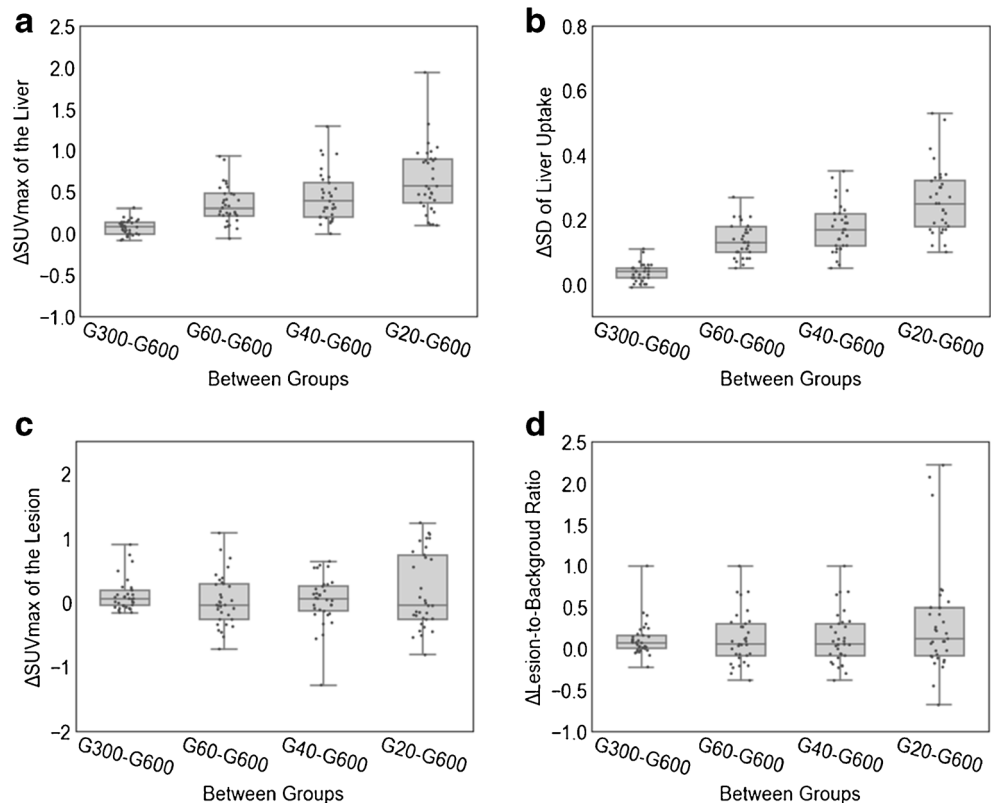
† The change of SUV_{max}, SD and lesion-to-background ratio (LBR) between the different groups were presented as s mean ± SD, using that of group 600 s as references

results at background obey the Poisson's distribution and the background feature is independent of acquisition time. Thus, the acquisition-time-dependent signal-to-noise ratio of PET image is directly proportional to SD. As the SD increases, the extremum value turns more dispersive, leading to SUV_{max} increases with shortening acquisition time.

Compared with the recommended regimen (with a time-activity-product [TAP] of 7 MBq/kg·min/bed, 6–10 bed per total-body scan) in the current guideline of the European Association of Nuclear Medicine for ¹⁸F-DG-PET/CT

oncological examination [1], elongating the axial FOV to 194-cm-long suggesting a theoretical minimization of ¹⁸F-DG regimen down to a TAP of 3.7 MBq/kg·min/bed (1 bed per total-body imaging). Upon the grade map of dose-and-time-dependent PET image quality, we suggest that an injected activity of 0.74 MBq/kg (estimated effective dose, 0.6–0.9 mSv) with an acquisition time of 5 min would be recommended for a routine protocol (Table 4 and Supplementary Table 4). The estimated effective doses of ¹⁸F-DG using total-body PET to acquire an optimal image

Fig. 2 Box plots showing the change of liver SUV_{max}, SD, lesion SUV_{max}, and lesion-to-liver ratio. The change of each metric was calculated as subtracting the value of G600s from that of G300 s, G60s, G40s, G20s in each patient. **a** The change in SUV_{max} of the liver increased gradually as the simulated dose was reduced. G60s-G600s, G40s-G600s, G20s-G600s were significantly higher than G300 s-G600s ($p < 0.05$). The difference was not significant between G60s-G600s and G40s-G600s ($p = 1$ with Bonferroni correction). **b** The SD of the liver uptake was significantly increased with simulated dose reduction ($p < 0.05$). **c, d** The difference of changes in SUV_{max} of the lesions and lesion-to-background ratio were not significant (all $p > 0.1$ with or without Bonferroni correction)



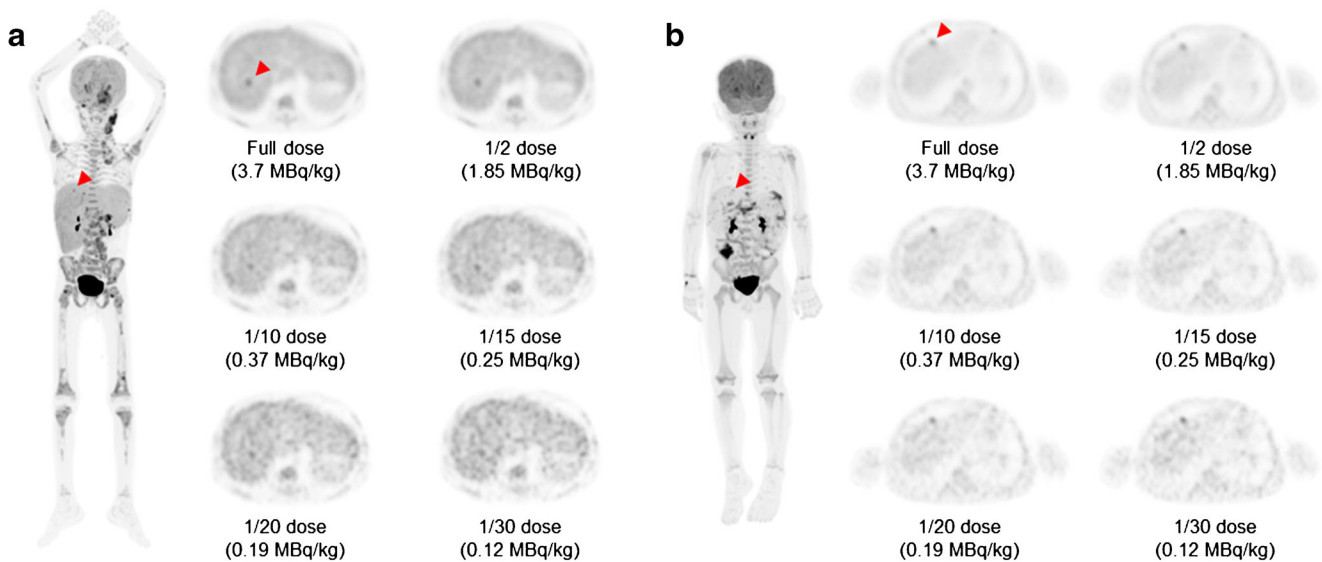


Fig. 3 MIP of the full dose image and axial view of the serial dose reduction image generated by reduced count. **a** An FDG-avid micro-lesion in the liver of a 7-year-old patient with neuroblastoma, with an SUV_{max} of 4.35 on the full-dose image. The lesion was identifiable as

reduced down to 1/20-dose; were un-diagnosable at 1/30-dose. **b** A micro-lesion in the subcapsular region of the liver in a 3-year-old patient with Burkitt Lymphoma was diagnosable in all dose reduction setting

ranging 0.3–0.9 mSv (injected activity 0.37–0.74 MBq/kg) were much lower than the ~4 mSv originated from a PET/MR examination (injected activity 1.8 MBq/kg) [10, 20, 21, 29, 30], making CT the major safety concern.

High-sensitivity-induced TAP reduction provides a particular opportunity in either low-dose PET imaging or quick scan. Our results illustrate an extreme reduction in either injected dose or acquisition time, namely, 0.25 MBq/kg × 10 min/bed or 3.7 MBq/kg × 0.67 min/bed, might be of use in special clinical scenarios, i.e., 0.25 MBq/kg for patients needing repetitive PET examinations through their disease course to manage the overall exposure or 0.67 min for patients who are claustrophobic or unable to keep still for minutes.

We concluded that the subjective image quality with an acquisition time of 40 s is comparable to that of clinical routine, which was different from the 60 s given by Zhang et al. [25]. Such difference was mainly brought by the difference in subjects’ BMI. Our study included pediatric patients with a BMI of $16.2 \pm 3.4 \text{ kg/m}^2$ (range, 12.2–22.2 kg/m^2), rather than adult patients with a BMI of $22.9 \pm 3.3 \text{ kg/m}^2$ (range, 18.4–28.9 kg/m^2) [25]. The quality of PET/CT images is inversely related to the subject’s fat mass, where the image quality of overweight patients often is degraded [31–33]. Besides, an acquisition time of 20 s showing an arguably diagnostic quality potentially reduces motion-induced artifacts decreases the length of sedation, improves patient comfort, and may better

Table 4 Image quality grading for time-activity product using total-body PET/CT (for pediatric dose study only)

Acquisition time (s [min])	Injected activity (MBq)										
	3.70	2.78	1.85	1.48	1.11	0.74	0.56	0.37	0.25	0.12	
600 [10]	1.00	0.75	0.50	0.40	0.30	0.20	0.15	0.10	0.07	0.03	
480 [8]	0.80	0.60	0.40	0.32	0.24	0.16	0.12	0.08	0.05	0.03	
300 [5]	0.50	0.38	0.25	0.20	0.15	0.10	0.08	0.05	0.03	0.02	
180 [3]	0.30	0.23	0.15	0.12	0.09	0.06	0.05	0.03	0.02	0.01	
120 [2]	0.20	0.15	0.10	0.08	0.06	0.04	0.03	0.02	0.01	0.01	
60 [1]	0.10	0.08	0.05	0.04	0.03	0.02	0.02	0.01	0.01	0.00	
40 [0.7]	0.07	0.05	0.03	0.03	0.02	0.01	0.01	0.01	0.00	0.00	
20s [0.3]	0.03	0.03	0.02	0.01	0.01	0.01	0.01	0.00	0.00	0.00	

*Green, recommended, optimal quality image can be obtained; Yellow and red, recommended under extreme conditions, suboptimal but diagnosable images can be obtained; Gray, not recommended, image obtained non-diagnostic

†Data are estimated proportion of time-activity-product, set full-dose×full-acquisition time (3.70 MBq/kg × 10 min/bed) as 1.00. The recommendation grade were given as follows, for proportion above that of full-dose×60s (0.10, subjective score 4+), green was given; for proportion above that of full-dose×40s (0.07, subjective score 3+), yellow was given; for proportion above that of full-dose×20s (0.03, subjective score 2+), red was given; for proportion below that of full-dose×20s (<0.03, subjective score <2), gray was given

‡Note that this card resulted from a proof-of-concept study, and intended to direct further dose investigation

assist radiation treatment planning [34]. If the acquisition time could be further reduced to an extreme that allows breath-holding PET/CT scan, respiratory motion mismatch between the PET data and the CT data could be avoided.

In our study, the overall image quality and the lesion conspicuity have been evaluated subjectively and objectively, while the lesion detectability was characterized by diagnostic accuracy. The lesion detection rate is strongly related to the image texture, the size, shape, and surrounding environment of the lesions and the reader's experience. As distinct from the phantom study, we compared the lesion detection rate between the count-reduced reconstructed image with that of G600s. When dose-reduction down to 0.12 MBq/kg (1/30-dose), the micro-lesion detectability decreased 3% (1/33). Note that the undiagnosable micro-lesion had a moderate FDG uptake in a background of tumor infiltrated liver segment (Supplementary Fig. 1), which was beyond diagnostic necessity. These results agree with previous studies that showed decreased detectability with the short acquisition protocol in adults and an anthropomorphic thoracic phantom with irregularly shaped lesion simulating inserts [25, 35–37]. However, the image quality of extreme low-dose may not be fully compensated by prolonged acquisition time. Because when acquisition time beyond a certain limit (i.e., 30 min) detected noise increases and may negatively impact the signal-to-noise ratio.

Limitations of this study include the small sample size, retrospective design, and restriction in extrapolation, i.e., limited to the total-body scanner. Particularly, the pediatric biodistribution of an extreme-low dose of ^{18}F -FDG remains unknown. Age-dependent or BMI-dependent image quality analysis has not been included due to the sample size. For lesion detectability, only micro-lesions were taken into account. The effects of low-dose images on lesion shape, volume, contrast, the impact of delayed imaging, and optimization of the reconstruction parameters warrant further investigation, where TAP might be further reduced by increasing the number of iterations and applying the Bayesian penalized-likelihood reconstruction algorithm.

Conclusion

The use of total-body PET/CT with 194-cm-long axial FOV might significantly decrease the administered dose while maintaining the image quality and diagnostic performance of micro-lesions in pediatric patients. Our data suggest that an optimal image quality superior to that of full-dose using conventional PET/CT can be achieved with an administered dose-reduction down to 0.37 MBq/kg (1/10th of the standard administered dose) using total-body PET/CT.

Supplementary Information The online version contains supplementary material available at <https://doi.org/10.1007/s00259-021-05304-4>.

Code availability The code applied during and/or analyzed during the current study are available from the corresponding author on reasonable request.

Authors' contributions Conceptualization: Xu Zhang, Wei Fan, Yu-Mo Zhao, Ying-Ying Hu; Methodology: Yu-Mo Zhao, Ying-Ying Hu, Wei-Guang Zhang; Formal analysis and investigation: Ying-Ying Hu, Yu-Mo Zhao, Tao Chen, Wei-Guang Zhang, Lin-Hao Wang; Writing - original draft preparation: Yu-Mo Zhao, Ying-Ying Hu, Tao Chen; Writing - review and editing: Ying-He Li, Yu-Mo Zhao, Jiatai Feng; Technical support: Jiatai Feng, Chenwei Li; Resources: Wei Fan; Supervision: Xu Zhang, Wei Fan, Ying-Ying Hu. All authors read and approved the final manuscript.

Funding The authors did not receive financial support from any organization for the submitted work.

Data availability The datasets generated during and/or analyzed during the current study are available from the corresponding author on reasonable request.

Declarations

Ethics approval All procedures performed in studies involving human participants were in accordance with the ethical standards of the institutional and/or national research committee and with the 1964 Helsinki declaration and its later amendments or comparable ethical standards.

Consent to participate Informed consent was obtained from legal guardians.

Consent for publication Additional informed consent was obtained from all legal guardians for whom identifying information is included in this article.

Conflict of interest Author JT.F. and CW.L. are employees of United Imaging Research. The other authors working at Sun-Yat Sen University Cancer Center have full control of the data and declare that they have no conflict of interest.

References

- Boellaard R, Delgado-Bolton R, Oyen WJ, Giammarile F, Tatsch K, Eschner W, et al. FDG PET/CT: EANM procedure guidelines for tumour imaging: version 2.0. *Eur J Nucl Med Mol Imaging*. 2015;42:328–54. <https://doi.org/10.1007/s00259-014-2961-x>.
- Townsend DW. Dual-modality imaging: combining anatomy and function. *J Nucl Med*. 2008;49:938–55. <https://doi.org/10.2967/jnumed.108.051276>.
- Fletcher JW, Djulbegovic B, Soares HP, Siegel BA, Lowe VJ, Lyman GH, et al. Recommendations on the use of ^{18}F -FDG PET in oncology. *J Nucl Med*. 2008;49:480–508. <https://doi.org/10.2967/jnumed.107.047787>.
- Chambers G, Froud R, Patel C, Scarsbrook A. ^{18}F -FDG PET-CT in paediatric oncology: established and emerging applications. *Br J Radiol*. 2019;92:20180584. <https://doi.org/10.1259/bjr.20180584>.
- Stauss J, Franzius C, Pfluger T, Juergens KU, Biassoni L, Begent J, et al. Guidelines for ^{18}F -FDG PET and PET-CT imaging in paediatric oncology. *Eur J Nucl Med Mol Imaging*. 2008;35:1581–8. <https://doi.org/10.1007/s00259-008-0826-x>.
- Fahey FH, Goodkind A, MacDougall RD, Oberg L, Ziniel SI, Cappock R, et al. Operational and Dosimetric aspects of pediatric PET/CT. *J Nucl Med*. 2017;58:1360–6. <https://doi.org/10.2967/jnumed.116.182899>.

7. Fahey FH, Treves ST, Adelstein SJ. Minimizing and communicating radiation risk in pediatric nuclear medicine. *J Nucl Med.* 2011;52:1240–51. <https://doi.org/10.2967/jnumed.109.069609>.
8. Sgouros G, Frey EC, Bolch WE, Wayson MB, Abadia AF, Treves ST. An approach for balancing diagnostic image quality with cancer risk: application to pediatric diagnostic imaging of ^{99m}Tc-dimercaptosuccinic acid. *J Nucl Med.* 2011;52:1923–9. <https://doi.org/10.2967/jnumed.111.092221>.
9. Treves TS, Gelfand M, Parisi M, Lassmann M, Goske M, Sexton-Stallone B, et al. Update: image gently and nuclear medicine at 10 years. *J Nucl Med.* 2019;60:7N–9N.
10. Parisi MT, Bermo MS, Alessio AM, Sharp SE, Gelfand MJ, Shulkin BL. Optimization of pediatric PET/CT. *Semin Nucl Med.* 2017;47:258–74. <https://doi.org/10.1053/j.semnuclmed.2017.01.002>.
11. Accorsi R, Karp JS, Surti S. Improved dose regimen in pediatric PET. *J Nucl Med.* 2010;51:293–300. <https://doi.org/10.2967/jnumed.109.066332>.
12. Alessio AM, Sammer M, Phillips GS, Manchanda V, Mohr BC, Parisi MT. Evaluation of optimal acquisition duration or injected activity for pediatric 18F-FDG PET/CT. *J Nucl Med.* 2011;52:1028–34. <https://doi.org/10.2967/jnumed.110.086579>.
13. Fahey FH, Goodkind AB, Plyku D, Khamwan K, O'Reilly SE, Cao X, et al. Dose estimation in pediatric nuclear medicine. *Semin Nucl Med.* 2017;47:118–25. <https://doi.org/10.1053/j.semnuclmed.2016.10.006>.
14. Poli GL, Torres L, Coca M, Veselinovic M, Lassmann M, Delis H, et al. Paediatric nuclear medicine practice: an international survey by the IAEA. *Eur J Nucl Med Mol Imaging.* 2020;47:1552–63. <https://doi.org/10.1007/s00259-019-04624-w>.
15. Treves ST, Falone AE, Fahey FH. Pediatric nuclear medicine and radiation dose. *Semin Nucl Med.* 2014;44:202–9. <https://doi.org/10.1053/j.semnuclmed.2014.03.009>.
16. Treves ST, Gelfand MJ, Fahey FH, Parisi MT. Update of the north American consensus guidelines for pediatric administered radiopharmaceutical activities. *J Nucl Med.* 2016;57:15n–8n.
17. Lassmann M, Biassoni L, Monsieurs M, Franzius C. The new EANM paediatric dosage card: additional notes with respect to F-18. *Eur J Nucl Med Mol Imaging.* 2008;35:1666–8. <https://doi.org/10.1007/s00259-008-0799-9>.
18. Koizumi K, Masaki H, Matsuda H, Uchiyama M, Okuno M, Oguma E, et al. Japanese consensus guidelines for pediatric nuclear medicine. Part 1: pediatric radiopharmaceutical administered doses (JSNM pediatric dosage card). Part 2: technical considerations for pediatric nuclear medicine imaging procedures. *Ann Nucl Med.* 2014;28:498–503. <https://doi.org/10.1007/s12149-014-0826-9>.
19. Vali R, Alessio A, Balza R, Borgwardt L, Bar-Sever Z, Czachowski M, et al. SNMMI procedure standard/EANM practice guideline on pediatric (18)F-FDG PET/CT for oncology 1.0. *J Nucl Med.* 2021;62:99–110. <https://doi.org/10.2967/jnumed.120.254110>.
20. Schmall JP, Surti S, Otero H, Servaes S, Karp JS, States LJ. Investigating low-dose image quality in whole-body pediatric 18F-FDG scans using TOF-PET/MRI. *J Nucl Med.* 2021;62(1):123–30. <https://doi.org/10.2967/jnumed.119.240127>.
21. Gatidis S, Schmidt H, la Fougère C, Nikolaou K, Schwenzer NF, Schäfer JF. Defining optimal tracer activities in pediatric oncologic whole-body (18)F-FDG-PET/MRI. *Eur J Nucl Med Mol Imaging.* 2016;43:2283–9. <https://doi.org/10.1007/s00259-016-3503-5>.
22. Cherry SR, Jones T, Karp JS, Qi J, Moses WW, Badawi RD. Total-Body PET: maximizing sensitivity to create new opportunities for clinical research and patient care. *J Nucl Med.* 2018;59:3–12. <https://doi.org/10.2967/jnumed.116.184028>.
23. Badawi RD, Shi H, Hu P, Chen S, Xu T, Price PM, et al. First human imaging studies with the EXPLORER Total-body PET scanner. *J Nucl Med.* 2019;60:299–303. <https://doi.org/10.2967/jnumed.119.226498>.
24. Zhang X, Cherry SR, Xie Z, Shi H, Badawi RD, Qi J. Subsecond total-body imaging using ultrasensitive positron emission tomography. *Proc Natl Acad Sci U S A.* 2020;117:2265–7. <https://doi.org/10.1073/pnas.1917379117>.
25. Zhang YQ, Hu PC, Wu RZ, Gu YS, Chen SG, Yu HJ, et al. The image quality, lesion detectability, and acquisition time of (18)F-FDG total-body PET/CT in oncological patients. *Eur J Nucl Med Mol Imaging.* 2020;47:2507–15. <https://doi.org/10.1007/s00259-020-04823-w>.
26. Liu G, Hu P, Yu H, Tan H, Zhang Y, Yin H, et al. Ultra-low-activity total-body dynamic PET imaging allows equal performance to full-activity PET imaging for investigating kinetic metrics of (18)F-FDG in healthy volunteers. *Eur J Nucl Med Mol Imaging.* 2021. <https://doi.org/10.1007/s00259-020-05173-3>.
27. Sekine T, Delso G, Zeimpekis KG, de Galiza Barbosa F, Ter Voert E, Huellner M, et al. Reduction of (18)F-FDG dose in clinical PET/MR imaging by using silicon photomultiplier detectors. *Radiology.* 2018;286:249–59. <https://doi.org/10.1148/radiol.2017162305>.
28. Seith F, Schmidt H, Kunz J, Küstner T, Gatidis S, Nikolaou K, et al. Simulation of tracer dose reduction in (18)F-FDG PET/MRI: effects on oncologic Reading, image quality, and artifacts. *J Nucl Med.* 2017;58:1699–705. <https://doi.org/10.2967/jnumed.116.184440>.
29. Alessio AM, Kinahan PE, Manchanda V, Ghioni V, Aldape L, Parisi MT. Weight-based, low-dose pediatric whole-body PET/CT protocols. *J Nucl Med.* 2009;50:1570–7. <https://doi.org/10.2967/jnumed.109.065912>.
30. Chawla SC, Federman N, Zhang D, Nagata K, Nuthakki S, McNitt-Gray M, et al. Estimated cumulative radiation dose from PET/CT in children with malignancies: a 5-year retrospective review. *Pediatr Radiol.* 2010;40:681–6. <https://doi.org/10.1007/s00247-009-1434-z>.
31. de Groot EH, Post N, Boellaard R, Wagenaar NR, Willemsen AT, van Dalen JA. Optimized dose regimen for whole-body FDG-PET imaging. *EJNMMI Res.* 2013;3:63. <https://doi.org/10.1186/2191-219x-3-63>.
32. Masuda Y, Kondo C, Matsuo Y, Uetani M, Kusakabe K. Comparison of imaging protocols for 18F-FDG PET/CT in overweight patients: optimizing scan duration versus administered dose. *J Nucl Med.* 2009;50:844–8. <https://doi.org/10.2967/jnumed.108.060590>.
33. Nagaki A, Onoguchi M, Matsutomo N. Patient weight-based acquisition protocols to optimize (18)F-FDG PET/CT image quality. *J Nucl Med Technol.* 2011;39:72–6. <https://doi.org/10.2967/jnmt.110.081661>.
34. Citrin DE. Recent developments in radiotherapy. *N Engl J Med.* 2017;377:1065–75. <https://doi.org/10.1056/NEJMr1608986>.
35. Matheoud R, Leva L, Secco C, Sacchetti G, Monica PD, Brambilla M, et al. Small lesions detectability with the biograph 16 hi-Rez PET/CT scanner and fast imaging protocols: performance evaluation using an anthropomorphic thoracic phantom and ROC analyses. *Ann Nucl Med.* 2011;25:179–88. <https://doi.org/10.1007/s12149-010-0437-z>.
36. Xie T, Bolch WE, Lee C, Zaidi H. Pediatric radiation dosimetry for positron-emitting radionuclides using anthropomorphic phantoms. *Med Phys.* 2013;40:102502. <https://doi.org/10.1118/1.4819939>.
37. Khamwan K, O'Reilly SE, Plyku D, Goodkind A, Josefsson A, Cao X, et al. Re-evaluation of pediatric (18)F-FDG dosimetry: Cristy-Eckerman versus UF/NCI hybrid computational phantoms. *Phys Med Biol.* 2018;63:165012. <https://doi.org/10.1088/1361-6560/aad47a>.